NASA Contractor Report 186023

A Computational Fluid Dynamics Analysis of the Hypersonic Flights of Pegasus

Darren Fricker, John Mendoza, and Ivan Catton
University of California, Los Angeles
405 Hilgard Avenue
Los Angeles, CA 90024

Prepared for
Dryden Flight Research Facility
Edwards, California
Under Cooperative Agreement NCC-2-374

1992

National Aeronautics and
Space Administration

Dryden Flight Research Facility
Edwards, California 93523-0273

CONTENTS

LIST OF FIGURES

ABSTRACT

The performance of a fully viscous, three-dimensional Navier-Stokes solver, PARC3D, was tested. The criteria for judging the performance of the CFD code were based on flight data from the first two flights of the Pegasus®. The flight data consisted of heat-transfer rates and sparse pressure coefficients primarily in the fillet region of the vehicle. The code performed remarkably well in all aspects of the tests. As expected, the best heat-transfer results were obtained for the low Mach number simulations. These results are attributed to the lack of high ablation rates at the lower Mach numbers since the CFD simulations did not account for ablation at the vehicle surface. As the Mach number increased, the ablative effects became more apparent in the comparisons. This effect was evident at the highest Mach numbers, when PARC3D would consistently overpredict the aerothermal heat flux. To evaluate the code thoroughly, flight data would be required over the entire fillet region, rather than at a few discrete locations. In this manner, CFD heat-flux profiles could be accurately evaluated. Although the pressure data were sparse, the trends suggest that the code predicts surface pressures with reasonable accuracy. Three of the four locations yield pressures that are consistent, but the CFD results yield pressures below the flight data by a factor of 2 at the fourth location.

Pegasus® is a registered trademark of Orbital Sciences Corp., Fairfax, Virginia.

LIST OF SYMBOLS

α	angle of attack, deg
δ_{ij}	Kronecker delta
λ	second coefficient of viscosity, slug/ft sec
μ	viscosity, slug/ft sec
ξ	computational coordinate directions
ρ	density, slug/ft^3
τ_{ij}	shear force, lb/ft^2
CFD	computational fluid dynamics
CPU	central processing unit
E	total energy per unit volume
F_j	inviscid flux vector
g	gravitational acceleration, ft/sec^2
G_j	viscous flux vector
HRSI	high-temperature reusable surface insulation
I	identity matrix
J	Jacobian transformation matrix
K	thermal conductivity, lb/°R sec
n	time step n
NASA	National Aeronautics and Space Administration
NEAR	Nielsen Engineering and Research, Inc.
P	pressure, lb/ft^2
Pr	Prandtl number
Q	conservation variable vector
q_j	heat flux in coordinate direction, lb/ft sec
q_{conv}	aerothermal heat flux at surface, Btu/ft^2 sec

Re	Reynolds number
t	time, sec
T	temperature, °R
T_{Suth}	Sutherland reference temperature, 198.6 °R
u_i	velocity in the Cartesian coordinate directions
X_j	Cartesian coordinate directions

INTRODUCTION

The determination of a hypersonic vehicle shape that optimizes aerodynamic loading and aerothermal heating is a most difficult and expensive design stage through which the concept vehicle must go. In the early years of aircraft design, this analysis entailed extensive wind-tunnel testing. As technology progressed and vehicles encountered more severe flight conditions, however, wind-tunnel simulation became expensive. Until recently, no alternative to wind-tunnel testing existed. But with the tremendous increase in the performance of computers over the last two decades, the field of computational fluid dynamics (CFD) has become a viable alternative. For complex, high-Mach-number fluid flows, large aerothermal heat loads are encountered because of the large viscous dissipation in the boundary layer. The high-temperature boundary layer also introduces variable fluid property effects. Thus, to obtain an acceptable CFD solution for these types of flow, the full Navier-Stokes equations must be solved. In addition, very fine grids must be used to resolve the boundary-layer flow, to capture shock waves, and to simulate other rapidly changing regions of the flow field. Previously, computations of this complexity were not even considered because of the memory limitations and the relatively slow speeds of the computers. Today, with the advent of sophisticated computers, fully viscous, three-dimensional solutions to the complete set of variable property Navier-Stokes equations can be feasibly generated using state-of-the-art algorithms.

Although the full set of Navier-Stokes equations are the basis for the CFD solutions, several assumptions are required to simplify the computations. Assuming that the Navier-Stokes equations can be factored in the coordinate directions and that the fluid behaves like an ideal gas with a constant Prandtl number are examples of such simplifications. Hence, the validity of the resulting CFD solutions must be checked. Code validation can be accomplished through two means. The first and easiest method is to simulate the flow numerically around some object under conditions that yield either an analytical or a well-understood solution. The results of the CFD code can then be compared with the known solution. The second code validation method is more complex and costly. This method involves simulating an actual flight condition for which flight data have been recorded. Code validation is a necessity if the CFD user is to have faith in the accuracy of the resulting solutions.

Normally, the first code validation method is chosen because of its simplicity. However, when flight data become available for complex flow conditions, a true test of a CFD code can be made. The simplest instrumentation for obtaining relevant flight data can be pressure taps, thermocouples, or heat-flux meters at the surface. Another method for obtaining qualitative information is particle injection, which relies on photography to visualize the flow field.

The Pegasus launch vehicle was instrumented by the National Aeronautics and Space Administration (NASA) Dryden Flight Research Facility to study hypersonic flow (ref. 1). Pegasus is used for launching multiple small satellites into orbit. The booster is carried underneath the wing of a B-52 in the same manner as was the X-15 hypersonic manned rocket. At an altitude of approximately 40,000 ft and at approximately Mach 0.85, Pegasus is dropped. After the initial free fall, the first-stage rocket engine ignites and a 2.5-g pullup follows. The vehicle soars to an altitude approaching 200,000 ft at Mach 8.0 where the first stage burns out. The first stage, which includes the wing and all control surfaces, separates

from the payload and the remaining rocket stages. The payload is then delivered to orbit by the remaining stages. The atmospheric flight of the first stage lasts approximately 80 sec.

The advantages of this configuration are numerous. Because of the initial altitude, the problems associated with high dynamic pressures and high heat fluxes at the lower altitudes are completely alleviated. The first-stage engine housing is outfitted with a delta wing and horizontal and vertical stabilizer tail surfaces. The all-movable tail surfaces are controlled by onboard computers, which allow the vehicle to use aerodynamic forces, rather than just thrust, to gain altitude and remain on the desired flight trajectory. Furthermore, the vehicle's first stage can be made much smaller since ignition does not occur until the vehicle is travelling at approximately Mach 0.85 at 40,000 ft. However, the obvious disadvantage is that a large aircraft is required to carry the launch vehicle before ignition. Thus, the size of the vehicle, and more importantly, the size of the satellites carried is limited.

Although very high dynamic pressures are not encountered during the Pegasus mission, complex flow patterns resulting from the high Mach numbers are present. High Mach numbers also result in significant aerodynamic heating. NASA Dryden instrumented Pegasus to study the heating caused by the wing shock intersection with the fillet boundary layer. Flight-1 instrumentation consisted of thermal measurement devices only, while flight-2 instrumentation added pressure sensors to the array of thermocouples and heat-flux meters. All instruments were located on the fillet and the upper and lower wing surfaces. By measuring the heat fluxes and pressures at the fillet sidewall, the shock location could be determined by noting the temperature and pressure jumps that occur across shock waves.

NASA Dryden was also interested in using hypersonic flight data to check the accuracy of state-of-the-art CFD codes. The Pegasus was the ideal vehicle for the CFD study since it was designed without the benefit of wind-tunnel testing. All aerodynamic design was based on CFD calculations performed by Nielsen Engineering and Research, Inc. (NEAR) (ref. 2). The preflight CFD solutions, as well as NEAR's postflight solutions (ref. 3) and the solutions presented in this thesis, yield a variety of CFD results from different codes for the NASA Dryden study.

THE CFD LABORATORY AND COMPUTATIONAL FACILITIES

The computational facilities available for this project included the UCLA Office of Academic Computing IBM 9000 (International Business Machines Corporation, Armonk, New York) supercomputer and IBM Risc System 6000 workstations. In addition to these university facilities, a private IRIS4D™ (Silicon Graphics, Inc., Mountain View, California) workstation and multiple PCs were used. The use of these machines as remote terminals allowed direct access to any UCLA computer as well as other off-campus systems.

The first stage of the project involved choosing which CFD code would best solve the Pegasus aerothermal heat-transfer and flow-field problem. For general simulation of this vehicle aft of the subsonic nose region, a thin-layer or parabolized Navier-Stokes code probably would suffice. However, the complexity of the flow in the fillet region caused by the wing shock interaction with the fillet boundary layer dictated that a code based on the fully viscous Navier-Stokes equations would be necessary to predict the heat flux at the surface accurately. Thus, PARC3D (ref. 4) was eventually chosen over the other contenders.

The code, as described in detail in the PARC3D user's manual (ref. 4), is a finite difference code based on the complete set of Navier-Stokes equations in conservation law form. Fully viscous, thin-layer, and Euler (inviscid) solutions can be calculated. A Baldwin and Lomax turbulence model (ref. 7) modified by Thomas (ref. 8) is available for turbulent flowfield calculations based on the Reynolds-averaged Navier-Stokes equations. Domain decomposition is supported in the most recent versions of the PARC code.

Once the code selection process was completed, the remainder of the tools necessary for performing CFD simulations was acquired. A grid-generation code is a necessary component of any functional CFD laboratory. For this purpose, two versions of the same grid-generation code were obtained. The code 3D INGRID runs on the IBM 9000 supercomputer, and GENIE3D is tailored to the IRIS4D workstation. These codes are interactive and can generate three-dimensional grids. They also allow for the creation of grids using algebraic methods or partial differential equation methods (elliptic solvers). Point clustering is accomplished through either exponential or hyperbolic tangent functions (ref. 5).

The third component necessary to complete the CFD laboratory involves flow visualization. For the most part, flow visualization was achieved with PLOT3D on the IRIS4D workstation (ref. 6). This code has very thorough documentation and was designed specifically for CFD use. The code PLOT3D offers 74 functions ranging from scalars, such as pressure coefficient, density, temperature, to vector functions, such as velocity, pressure gradients, and density gradients.

THE PEGASUS SIMULATIONS

The first step in the CFD process was to obtain a computational grid of the Pegasus vehicle and the surrounding space that could be used in the finite difference solution code, PARC3D. A computational grid is the set of points that are strategically placed on the boundaries of the flow channel and distributed in the space between the boundaries. These points are packed more densely in areas that exhibit complex flow patterns or sharp gradients and are structured so that "the indices can be formally considered as coordinates of a curvilinear coordinate system with nonvanishing Jacobian" (ref. 4). Since CFD work involving the Pegasus vehicle had been done previously by NEAR (ref. 2) under the direction of NASA Dryden, arrangements were made for the acquisition of their computational grid. Furthermore, since the region of interest was ahead of the wing trailing edge, only the front part of the grid was used. Thus, the flow field around the tail surfaces was not calculated. Simulating only the front part of the vehicle can be done when the flow speed exceeds the speed of sound since the downstream disturbances cannot propagate forward to affect the upstream flow field. The front section had 92 points in the axial direction, 83 points in the angular direction, and 51 points in the radial direction extending from the vehicle surface to the free stream for 384,436 total grid points (fig. 1). This grid was used for the first simulation, but was later modified to include 451,686 total grid points (fig. 2).

To determine which conditions would be simulated, the flight-1 trajectory was used. The trajectory data correlated the Mach number and angle of attack as a function of the altitude. Weather balloon data were used to determine the free-stream reference conditions as a

function of altitude. The two flight conditions chosen for simulation were Mach 3.52 with an angle of attack of 7.35° and Mach 6.67 with a 0° angle of attack.

Since the PARC code is primarily a steady-state flow solver and only two flight conditions were being simulated, the underlying assumption was that the aerodynamics could be treated as if they were steady even though the vehicle was accelerating through the profile. This assumption of quasi-steady-state aerodynamics is widely used in the CFD community and is based on the fact that the flow field adapts at a very fast rate to changes in free-stream conditions as the vehicle is accelerating. This is in contrast to the solid-side temperature profile which gradually changes throughout the flight, never reaching steady state.

The purpose of performing flight-1 simulations was to evaluate the capability of a CFD code to accurately predict the heat-transfer rates to the surface of the vehicle in regions of complex flow. It was also desired to determine if the code could predict the location of the wing shock intersection with the fillet, which forms the intersection of the cylindrical body with the flat wing.

Pegasus flight 1 was instrumented with various heat-flux gauges and thermocouples around the fillet region and the leading edge of the wing. Shuttle-tile high-temperature reusable surface insulation (HRSI) plugs were used to measure the surface temperature from which the convective heat flux could be obtained. These gauges have well-known properties and generally yield accurate results. The problem with these measurements was that the surface temperature of the vehicle was different from the surface temperature of the plugs, since an ablative layer covered the entire vehicle skin except the plug surface. Thus, the resulting heat fluxes to the plugs and that to the rest of the vehicle would differ. Thermocouples buried underneath the ablative surface were also used to collect data. The orientation of the thermocouples varied from a single thermocouple placed between two of the thermal protection system layers to thermocouple stacks, which had up to three thermocouples in line, with each thermocouple placed between the layers of the thermal protection system. The thermal protection system was composed of an ablative layer, a brittle foam layer and the graphite-epoxy skin. The most usable thermocouple data were obtained when a thermocouple was placed between the ablative and foam layers, between the foam and graphite-epoxy skin layers, and behind the graphite-epoxy skin. These thermocouple stacks allowed the use of inverse heat conduction codes to estimate the magnitude of heat transfer. These inverse conduction results were only approximate because ablation effects were not included in the analysis (ref. 9). The ablative materials used were Firex RX-2376A (Pfizer Minerals, Pigments and Metals Division, New York, New York) and Thermolag T-230 (Thermal Science, Inc., St. Louis, Missouri), which have ablation temperatures of 250 and 230 °F, respectively. The isothermal surface temperature for the CFD calculations was assumed to be the ablation temperature since no thermocouples could be placed on the receding surface. Finally, when only given temperatures underneath the surface and no instrumentation to record the surface recession rate, the heat flux consumed by ablation is unknown.

The second flight of the Pegasus vehicle offered slightly different instrumentation to check the validity of the CFD solutions. Although the thermal instruments were of the same design, pressure taps were included at various locations around the fillet. The taps allowed for direct comparison of the pressures from flight data and the CFD solutions without any intermediate complicated analysis of flight data, which might have introduced its own errors.

Since the ablation rates were low and the CFD solutions did not account for ablative products in the boundary layer, any effect of ablation on the measured pressures was ignored.

Again trajectory data were used in determining the conditions to be simulated. Three flight conditions were chosen that represent various regimes of the flight profile. These conditions were at Mach numbers of 3.52, 5.0, and 6.67 corresponding to angles of attack of 2.65°, 0.5°, and 0°, respectively. The Mach number of 3.52 was also simulated for flight 1 but at a much larger angle of attack. Similarly, the Mach 6.67 case was also simulated based on flight-1 trajectory data. The only difference between the two simulations at Mach 6.67 was the free-stream reference conditions. The Mach-5.0 simulation was previously performed by NEAR, allowing Dryden to make a direct comparison of the results of the two codes.

The focus of the flight-2 simulations was expanded toward validating whether the CFD code could accurately predict both the pressure coefficient and the surface heat flux at the instrument locations. The region of interest was again the fillet sidewall under the leading edge of the wing. Pressure gauges were placed in this region with the goal of determining the intersection of the wing shock with the fillet. The test for the CFD code was for it to determine the appropriate intersection location as well as the correct magnitudes of the pressure coefficients and the heat-transfer rates.

RESULTS AND DISCUSSION

The first simulation completed was at Mach 3.52 and an angle of attack of 7.35°. Reference conditions were taken from the flight-1 trajectory data. The second flight-1 condition, Mach 6.67 with 0° angle of attack, was simulated simultaneously. It became apparent, however, after viewing the solution between iterations with PLOT3D, that the solution in the nose region of the vehicle was not converging. This nonconvergence was also observed when monitoring the heat flux at the stagnation point. Rather than converging to a single value, the heat flux oscillated randomly. Since the PARC code only allows the conservation variables to change by a prescribed percentage during each iteration (10 percent for these simulations), many iterations were required for the fluctuations to complete a cycle. The heat fluxes varied by as much as a factor of 10 in as few as 800 iterations. The pressure coefficient contours at the nose surface, as shown by PLOT3D, displayed a star-like pattern around the stagnation point. Because of the symmetry of the vehicle in the nose region, especially when at zero angle of attack, this star pattern was unexpected, and thus was assumed to be nonphysical.

To discern whether the problem was associated with the grid or the CFD code, the nose region was separated from the remainder of the grid and the number of grid points in the nose region was tripled. The two nose grids were then tested to see if a similar solution resulted regardless of grid density. Upon inspection of the solutions, the coarse grid solution was observed to remain with the star-like pattern while the fine grid solution was observed to yield a symmetric pressure coefficient pattern, as was originally expected. Thus, it was concluded that the problem was completely the result of having too coarse of a grid in the nose region. Because of this, the dense nose grid was used for the remainder of the cases simulated.

Rather than simulating the nose region again for the flight-1 Mach 6.67 condition, the already completed nose solution was input to the remainder of the grid (fig. 2). This was accomplished by using the solution located two grid surfaces from the outflow boundary of the nose grid as a fixed inflow boundary condition for the back part of the grid. This procedure is essentially a manual domain decomposition.

During the domain decomposition, an interesting trend was observed. Faster convergence rates were observed when separating the nose region from the remainder of the grid even after accounting for the difference in the number of grid points. A 16-percent decrease in overall central processing unit (CPU) time was observed simply by separating the two regions of flow. Although more direct investigation will be required to understand this phenomenon fully, it is currently believed that the increase in performance was because of the distinctly different types of flow in each region. The flow in the nose region was dominantly subsonic since the bow shock was nearly normal to the free stream. As the flow accelerated around the vehicle, it became supersonic. Even as the flow passed through the wing shock it remained primarily supersonic because of the shock's obliqueness. Thus, for the most part, the only subsonic flow in the rearward section of the grid was in the boundary layer. The significance of the flow being either subsonic or supersonic lies in the differing types of partial differential equations that describe the two flow regimes. Subsonic flow is characterized by elliptic partial differential equations whereas supersonic flow is characterized by hyperbolic partial differential equations. Boundary-layer flow is described by parabolic equations. Typically, each type of equation is best solved by its own unique method.

It is currently believed that the increase in performance was observed because the grid was split so that the flow in each part was predominantly characterized by either elliptic or hyperbolic equations. The only requirement on splitting the grid was to ensure that the outflow from the nose grid was supersonic. Thus, disturbances in the flow in the back part of the grid could not travel upstream, reflecting off the inflow boundary. For all simulated flight conditions, the flow through the outflow boundary of the nose grid was entirely supersonic, except for the subsonic boundary layer. Since the back part of the grid contained the majority of grid points and the flow in this region was almost completely supersonic, the equations governing the flow were predominantly hyperbolic. Thus, an increase in performance was observed. Because of the lower CPU time required, the remainder of the simulations was performed in a similar manner.

To help the user determine the convergence of a solution, the PARC code calculates a relative measure of error (L2-residuals) after each iteration. A sample of L2-residuals from one of the simulations is shown in figure 3. On average, approximately 50 hr of CPU time on the IBM 9000 supercomputer is required to complete each simulation. The number of iterations required varies from about 4000 to 7000.

Usable flight data were obtained from 10 HRSI plugs during flight 1 and 8 plugs during flight 2. The flight-1 plugs recorded only thermal measurements for use in determining the convective heat transfer (fig. 5). The flight-2 plugs recorded thermal data in the same manner, but four plugs were also outfitted with ports to measure pressures (fig. 6). The thermal data obtained during the two flights were fairly consistent. Thus, it is likely that the HRSI plugs yield accurate data. An estimation of the errors associated with the measurements yields $q_{conv} = \pm 22.6$ percent (ref. 1). However, since the plugs were not covered with an ablative layer as was the rest of the vehicle surface, the surface temperatures and

properties of the plugs differed from those of the vehicle surface. These discrepancies result in differing heat-transfer rates. The heat flux into the ablative layer was not actually measured because of the difficulty of placing thermocouples on a receding surface.

Another possible source of error in the flight data involved the method in which the radiative heat flux was estimated. It was assumed that the plug radiated to free space, yielding a component of radiation $q_{rad} = \varepsilon\sigma T_s^4$ (ref. 1). Given the limited data and the uncertainty of the composition of the boundary layer, this was the best estimate possible. However, when in the hypersonic flight regime, this method of radiation estimation does not always hold true. Because of the high temperatures in a hypersonic boundary layer and the usual occurrence of dissociated air molecules and products of ablation within the boundary layer, a component of radiative heat transfer is in the direction from the fluid to the vehicle surface (ref. 10 and fig. 4). Ignoring the boundary-layer radiation component is valid for supersonic flows, since no dissociation of the air occurs and no ablative products are found in the boundary layer. For this case, the emissivity of the boundary layer is essentially zero, allowing all surface radiation to pass through the boundary layer. However, hypersonic, chemically reacting boundary layers typically have an emissivity greater than zero, with the magnitude depending on the properties of the products of ablation and the extent of the air dissociation. Thus, a component of radiation can be directed into the vehicle surface.

Other discrepancies developed as assumptions were made in the CFD analysis. The boundary condition at the surface of the vehicle was assumed to be no-slip, isothermal. Thus, the entire vehicle surface temperature was prescribed to be the ablation temperature. In reality, hot and cold spots would exist on the surface, changing the local heat-transfer rates. Furthermore, the CFD solutions were also calculated ignoring ablation. The products of ablation in the boundary layer and the effects of blowing at the wall were not included. These assumptions directly affect the resulting heat-transfer rates.

It has been suggested that by setting the local surface temperatures in the CFD analysis to the values measured with flight instrumentation, more accurate local heat-transfer rates would result. These local modifications were not done in this study because the primary goal was to determine the CFD code's ability as a predictor of flight data. In general, flight data will not be available for use as boundary conditions; in which case, a best guess must be made for the surface temperature. The best guess for the Pegasus simulation was setting the surface temperature equal to the ablation temperature everywhere.

Because of the scarcity of the flight data and the assumptions made in the CFD analysis, expecting the CFD predictions to match flight measurements identically would be optimistic. Considering the various assumptions, the data compare remarkably well (figs. 7 - 16). However, because of the many sources that could lead to discrepancy between the two data sets, it was decided that the data might be better analyzed by nondimensionalization with a certain reference heat flux at a prescribed location. As shown in figure 5, the farthest forward and lowest HRSI plug was used as the reference (plug 7). This plug was chosen as a reference free-stream heat flux because it was positioned so that it would always be ahead of the wing shock. The nondimensional results display some interesting trends (figs. 8-16).

When comparing figures 7 and 8, which both correspond to flight 1 at Mach 3.52, one may wonder why the magnitudes of the heat fluxes vary so distinctly yet the relative heat

fluxes are so similar. The most feasible explanation of this becomes apparent when it is realized that this simulation is relatively early in the flight. Thus, the surface temperature in the fillet region might not have reached the ablation temperature, as was prescribed in the CFD analysis. If this were the case, the CFD solution would underpredict the heat flux. An underprediction is exactly what is observed (fig. 7). Support for this argument is gathered when examining the plot of relative heat fluxes at the same flight condition (fig. 8). The plot suggests that the CFD code predicts the areas of high and low heating as recorded by the flight instrumentation.

The opposite trend is observed when comparing figures 9 and 10, which correspond to flight 1 at Mach 6.67. The CFD predictions for heat transfer at all HRSI plugs are larger than the measured values. This too can be attributed to the assumptions associated with the CFD simulations. Since this condition occurred late in the flight, the layers of the vehicle's thermal protection system would have all heated up. The surface temperature would have reached the ablation temperature and the ablation rate probably would be at its highest level. Because of the higher temperatures of the vehicle's thermal protection system layers, the conduction heat resistance would have increased. Thus, most aerothermal heating during the last part of the flight would have been dissipated by ablation. As known from mass transfer rate theory, the boundary-layer thickness increases with increasing ablation rates. The thicker boundary layer thus decreases the heat-transfer rate to the surface. Since the CFD simulations ignore ablation, it would be expected that the CFD predictions would be higher than the actual flight measurements. Again, it can be seen that although the magnitudes differ, the relative heat fluxes (fig. 10) compare well. This suggests that the CFD code predicts the areas of highest and lowest heating as was observed by flight data.

The heat-transfer rates for flight 2 at Mach 3.52 compare best with flight data than all other results (figs. 11 and 12). All heat-flux magnitudes lie well within the accuracy of the flight data. As with the results for flight 1 at Mach 3.52, the relative heat fluxes compare remarkably well. That the magnitudes of the heat fluxes compare so favorably, which was not true for magnitudes for flight 1 at Mach 3.52, suggests that the surface temperature of the vehicle during flight 2 at Mach 3.52 had risen close to the ablation temperature. Because of the assumptions made in the flight data analysis and those in the CFD simulations (treating hypersonic flow as supersonic flow), it was expected that the best heat-transfer results would be obtained at the lower Mach numbers. This trend was definitely observed.

The flight-2 at Mach 5.0 results show some discrepancy with flight data (figs. 13 and 14). This was the only simulation that yielded results that were not easily explained by a simple analysis of the underlying assumptions. The results suggest that the ablation rates were probably not too large at these flight conditions. This assumption is made because the CFD heat-transfer predictions are neither consistently too high nor too low. Rather, near the bottom of the fillet, the CFD heat-transfer rates lie almost completely within the uncertainty of the HRSI instrumentation measurements. However, the CFD heat-transfer results near the top of the fillet directly underneath of the wing are approximately 40 percent lower than the measured values. The same trend is observed when comparing the relative heat fluxes (fig. 14). This cooler region can be seen when observing the temperature contours. Because of the relative scarcity of flight data, it is difficult to assess the origin of the problem. However, it appears that the CFD code incorrectly predicts this cooler region.

The aerothermal heating results for flight 2 at Mach 6.67 (figs. 15 and 16) show the same basic trends as those for flight 1 at Mach 6.67. The CFD code again overpredicts the surface heat fluxes, although not as greatly as the flight-1 simulation. Similar to the previous analysis, this overprediction can be attributed to the high ablation rates that were probably present during this part of the flight profile. Although the relative heat fluxes do not compare as well as they did for the flight-1 simulation, the results are satisfactory. The majority of the discrepancy is because the CFD code drastically overpredicted the reference heat flux. Thus, the CFD relative heat fluxes appear low.

Similar to the heat-transfer results, the pressure data yield a few identifiable trends (figs. 17 - 20). However, drawing conclusions about the accuracy of the CFD code in predicting pressure is nearly impossible because of the scarcity of the data. Pressure data were only recorded during flight 2, and only four of the HRSI plugs on the fillet were outfitted with pressure sensors. Also, the pressure data are inaccurate beyond about Mach 5 because of the extremely low pressures encountered. Thus, only two of the five flight conditions provide pressure data for a comparison.

The two simulations, flight 2 with Mach numbers of 3.52 and 5.0, show the same trend. The pressure correlates excellently at HRSI plugs 5 and 7 and reasonably well at HRSI plug 9. However, HRSI plug 8 underpredicts the pressure by approximately a factor of 2 at both Mach numbers. More flight data would be needed to determine the source of the discrepancy.

Another flow parameter of interest was to determine if the wing shock intersected the fillet, and if so, at what location. Before the CFD solutions were completed, it was questioned whether the wing shock would intersect the fillet. It is commonly known that when fluid flows through a rectangular channel, a vortex in the corner is present. It was suggested that this swirling motion might neutralize the shock before it reached the fillet. Apparently, this argument is correct. The CFD solutions confirm that the shock does not reach the fillet for any of the flight conditions. Whether the vortex is entirely responsible for the shock's dissipation is also a matter for cogitation. The artificial viscosity used in the PARC3D code could be partially responsible for the dissipation of the shock. However, the artificial viscosity cannot be eliminated completely since it is used to eliminate spurious oscillations near shock discontinuities. To determine whether the dissipation is physical or a result of the artificial viscosity, it is necessary to replace the artificial viscosity with a nonlinear filter (ref. 11). This will be the subject of future work.

CONCLUSIONS AND FUTURE WORK

Once the initial grid problems were resolved, the PARC3D computation fluid dynamics (CFD) code performed remarkably well in predicting the general flow field around the Pegasus vehicle. The best heat-transfer results were consistently obtained when simulating the lower Mach numbers. This was expected since the ablation rates were smaller at the lower Mach numbers. As the Mach number was increased, the effects of the higher ablation rates were seen in the data. The CFD code, which ignores ablation, predicted higher heat-transfer rates than those that were measured. This was attributed to the thickened boundary layer caused by ablation that would have been present during the flight measurements. The

thickened boundary-layer leads to smaller gradients, and thus, smaller heat-transfer rates. Therefore, it was natural to expect the CFD code to predict too high of a heat-transfer rate.

It was also concluded that a better method of looking at the data was to nondimensionalize it by using a reference heat flux at a prescribed location. Using the relative heat fluxes for comparison eliminates the effects of ablation when analyzing the data. By comparing the data in this fashion, it was determined whether the code could accurately predict the regions of high and low heat transfer. This method of presenting the data proved that, in general, the code performed remarkably well in determining the relative intensity of the aerothermal heating.

The pressure comparisons were limited because of the scarcity of flight data. Pressure measurements were available for only two of the five simulations and at only four fillet locations. Thus it was impossible to draw many conclusions regarding the accuracy of the CFD code in predicting pressure. However, the CFD predictions for pressure were very good at three of the four locations for both flight conditions. The fourth location showed a factor of 2 discrepancy for both simulations, with the CFD pressures being lower than those measured.

Another interesting fact that needs more investigation involved the 16-percent decrease in computational time required when the nose region was separated from the remainder of the flow field. This was attributed to the differences associated with the partial differential equations that describe the two types of flow most prevalent in each region. The nose region was largely subsonic, which is described by elliptic partial differential equations, whereas the back part of the flow field was largely supersonic, which is characterized by hyperbolic equations. The boundary layer in both regions is described by parabolic partial differential equations.

Future work associated with aerothermal heating of the Pegasus includes analyzing the heat-transfer rates to the leading edge of the wing. This will be done after the Pegasus is flown with a nonablating glove that fits over the leading edge. Incorporation of a better turbulence model into the code also will be done since flight data yielding the location of turbulence transition are expected from the glove experiment. The most important modification to the PARC3D code, which is being performed, will be the addition of a nonlinear filter to replace the artificial viscosity (ref. 11). It is hoped that this filter will provide improved shock capturing and local heat-transfer rate prediction. Once the filter is incorporated, tests regarding the wing shock intersection with the fillet will be continued to determine the exact cause of the dissipation of the shock wave.

A computational strategy is also being developed for future CFD work. Since the code requires a large amount of central processing unit time to reach convergence, improvements associated with speed are desired. It is believed that by analytically solving for the flow field in the elliptic region directly behind the bow shock and superimposing this solution with the CFD computation, a great increase in performance will result. The addition of the nonlinear filter also should result in decreased computational time. By accurately locating the shock early in the convergence cycle and eliminating the oscillations after each iteration near the shocks without modifying the Navier-Stokes equations with artificial dissipation, better solutions should result in fewer iterations.

Overall, PARC3D performed exceptionally well in predicting the boundary-layer heat fluxes and pressures at the locations of the sensors. Whether the code predicts the proper values at other locations can only be extrapolated from its performance in the fillet region since data were only recorded at the fillet surface. Although the data for comparison are limited, the general trends suggest that the PARC3D code is a sufficient tool for the thermal design analysis of a concept vehicle.

ACKNOWLEDGEMENTS

The research presented in this paper was fully supported by NASA Dryden Flight Research Facility under contract No. FDP NASA/A NCC-2-374. Special thanks go to Robert E. Curry and Gregory K. Noffz of NASA Dryden for their many helpful discussions and insights.

REFERENCES

1. Noffz, Gregory K., Curry, Robert E., Haering, Edward A., Jr., and Kolodziej, Paul, *Aerothermal Test Results From the First Flight of the Pegasus Air-Launched Space Booster*, NASA TM-4330, 1991.

2. Mendenhall, Michael R., Lesieutre, Daniel J., Caruso, Steven C., Dillenius, Marnix F. E., Kuhn, Gary D., Aerodynamic Design of Pegasus™: Concept to Flight with CFD, Missile Aerodynamics, AGARD-CP-493, 1990.

3. Kuhn, Gary D., Post-Flight Aerothermodynamic Analysis of Pegasus™ Using CFD Techniques, NEAR TR 423, Nielsen Engineering and Research, Inc., June 1991.

4. Cooper, G. K. and Sirbaugh, J. R., PARC Code: Theory and Usage, AEDC-TR-89-15, Arnold Engineering Development Center, Dec. 1989.

5. Dorrell, E. W., Jr. and McClure, M. D., 3D INGRID: Interactive Three-Dimensional Grid Generation, AEDC-TR-87-40, Arnold Engineering Development Center, April 1988.

6. Walatka, Pamela P., Buning, Pieter G., Pierce, Larry, and Elson, Patricia A., PLOT3D User's Manual, NASA Ames Research Center, Moffett Field, March 1990.

7. Baldwin, B. S. and Lomax, H., Thin Layer Approximation and Algebraic Model for Separated Turbulent Flows, AIAA-78-257, AIAA 16th Aerospace Sciences Meeting, Huntsville, Alabama, January 1978.

8. Thomas, P. D., *Numerical Method for Predicting Flow Characteristics and Performance of Nonaxisymmetric Nozzles - Theory*, Langley Research Center, NASA CR-3147, September 1979.

9. Mendoza, J., Fricker, D., and Catton, I., Inverse Heat Conduction in a Planar Slab Composed of Multiple Material Layers, being reviewed for ASME National Heat Transfer Conference, San Diego, 1992.

10. Anderson, John D., Jr., *Hypersonic and High Temperature Gas Dynamics*, McGraw-Hill Book Company, New York, 1989.

11. Engquist, Bjorn, Lotstedt, Per, and Sjogreen, Bjorn, Nonlinear Filters for Efficient Shock Computation, *Mathematics of Computation*, Vol. 52, No. 186, Apr. 1989, pp. 509-537.

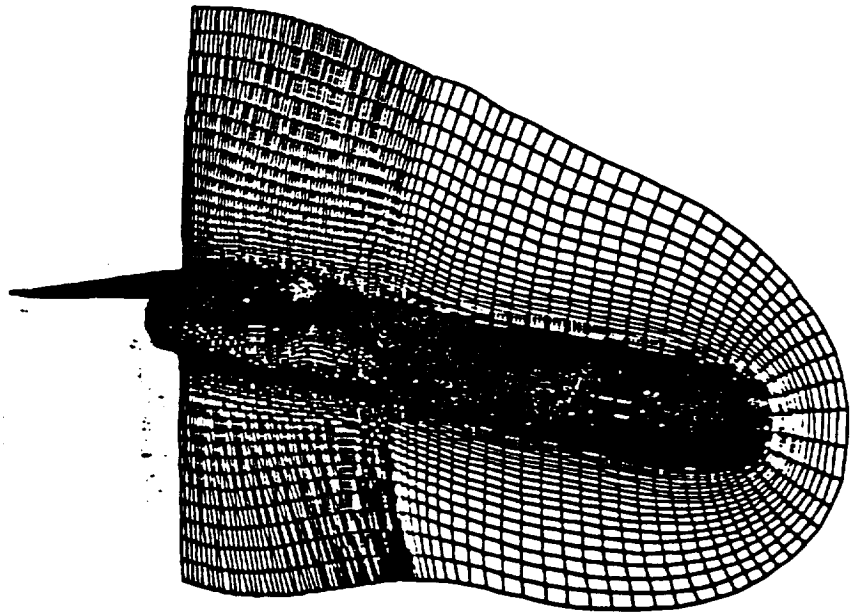

Figure 1. Original computational grid boundaries.

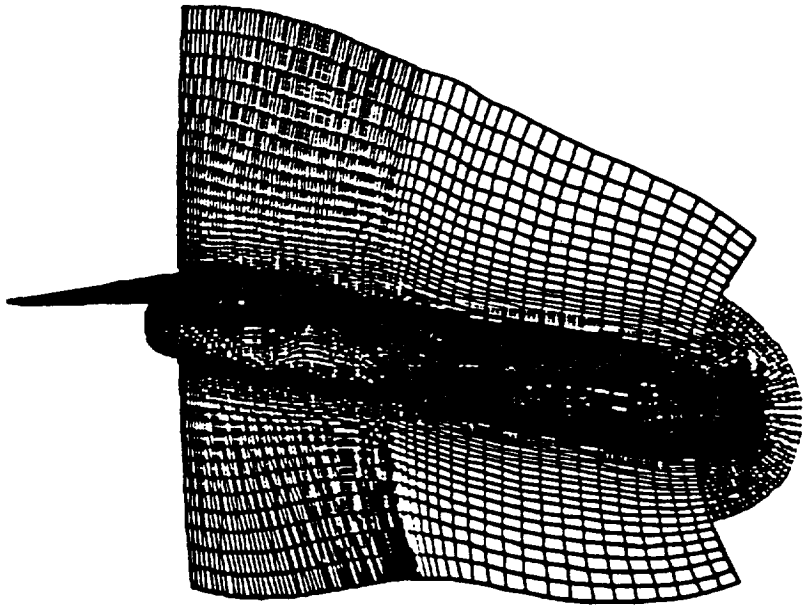

Figure 2. Modified computational grid boundaries.

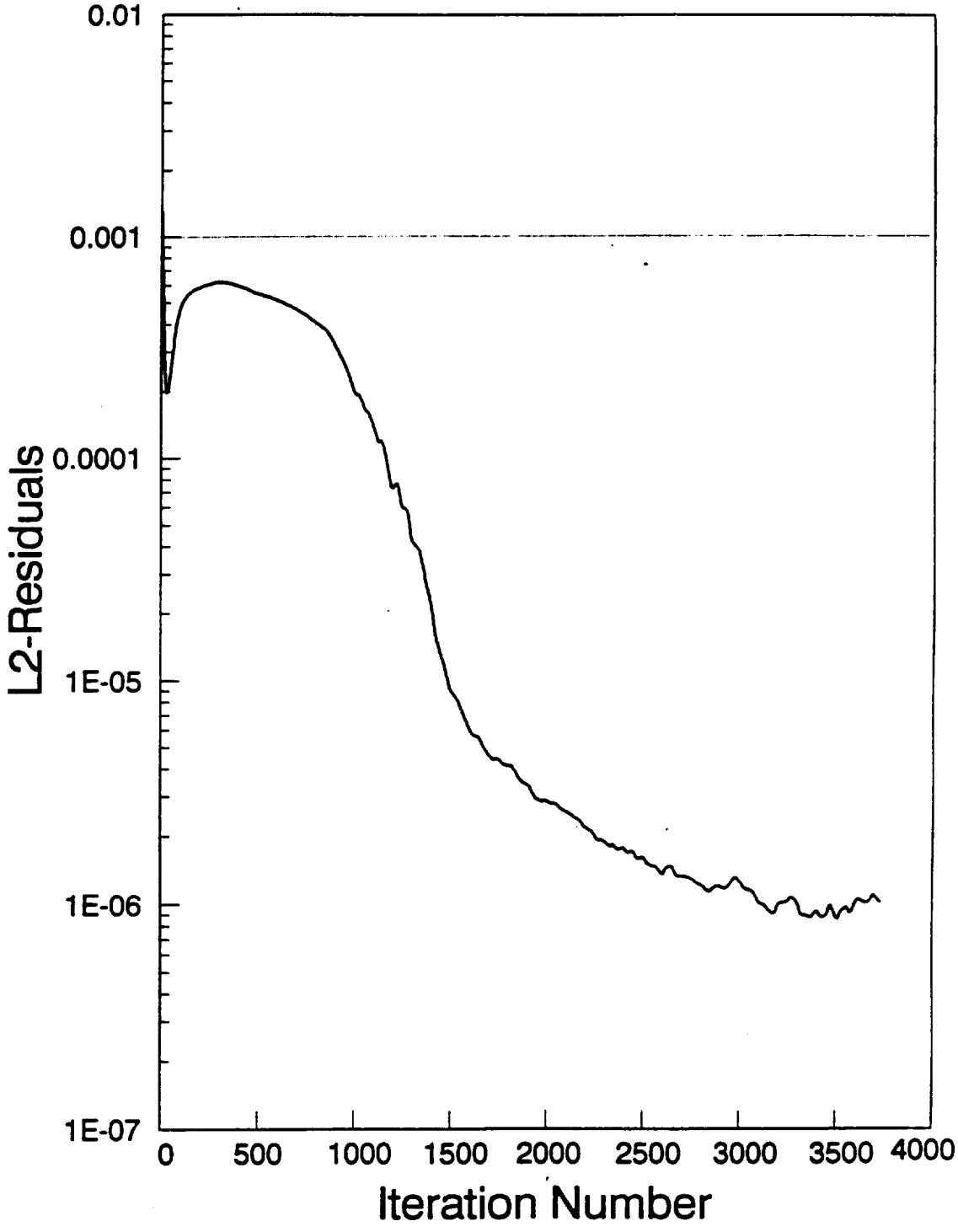

Figure 3. Sample plot of L2-residuals.

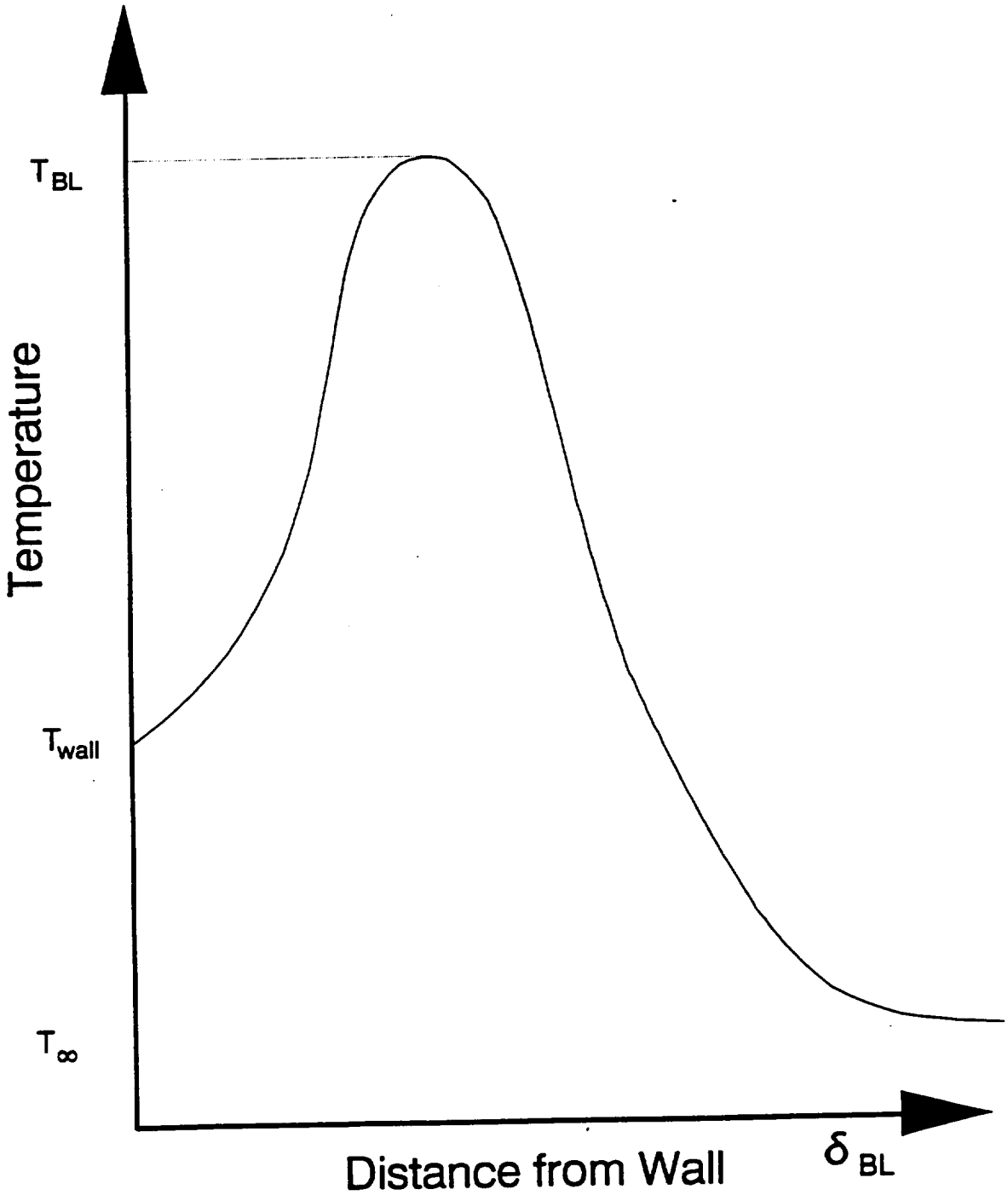

Figure 4. Hypersonic boundary-layer temperature profile.

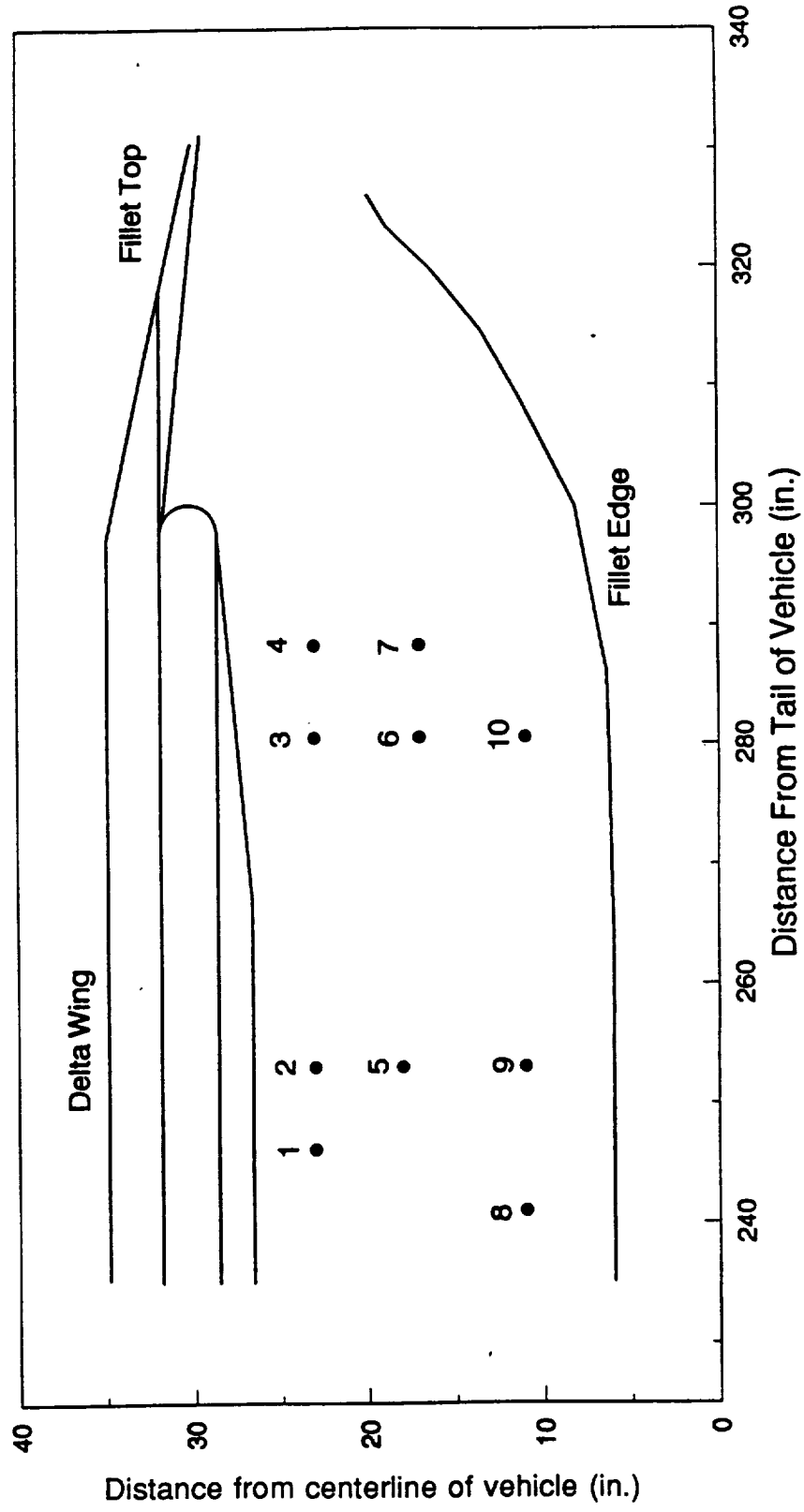

Figure 5. Flight-001 instrumentation locations.

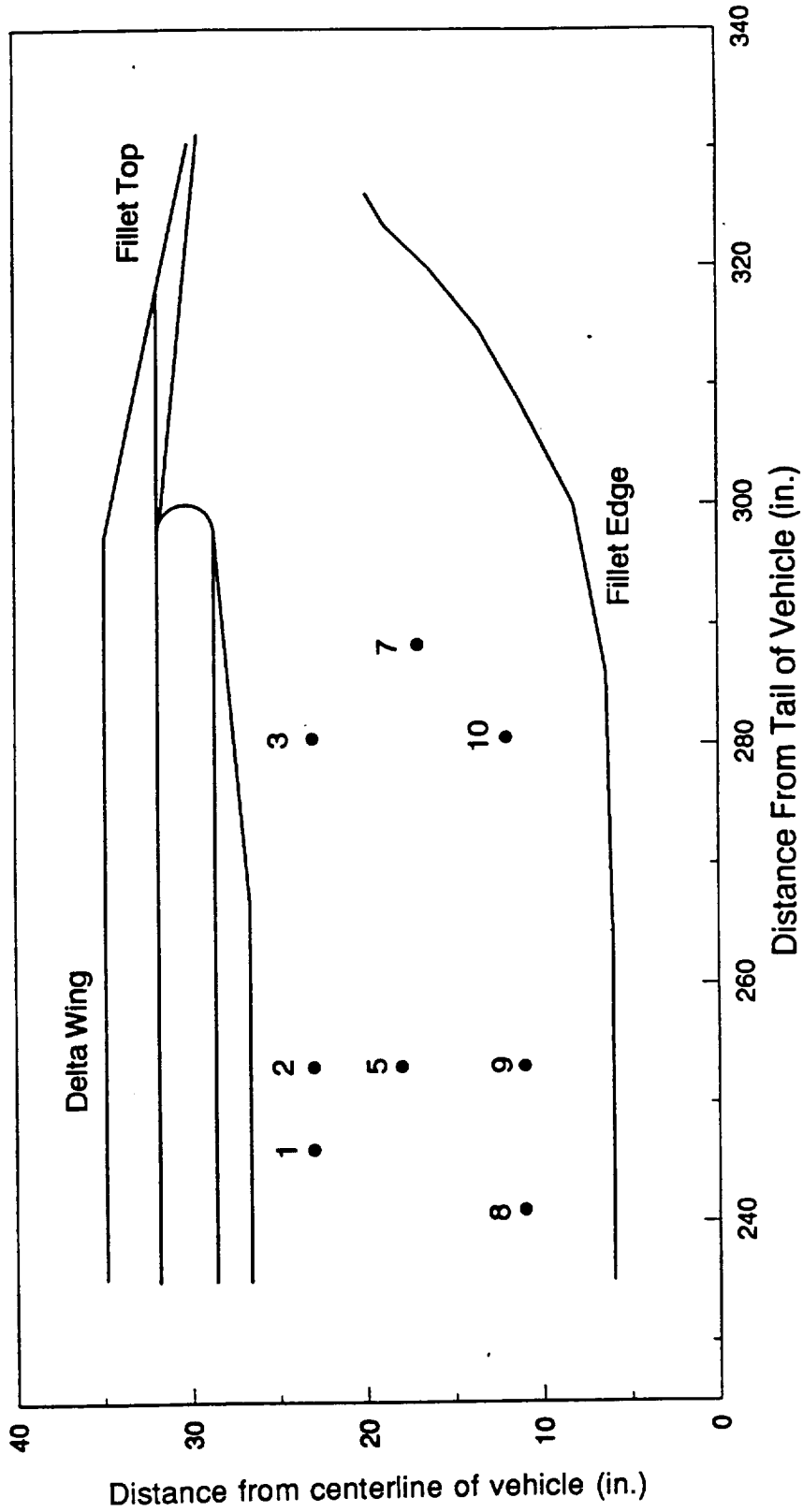

Figure 6. Flight-002 instrumentation locations.

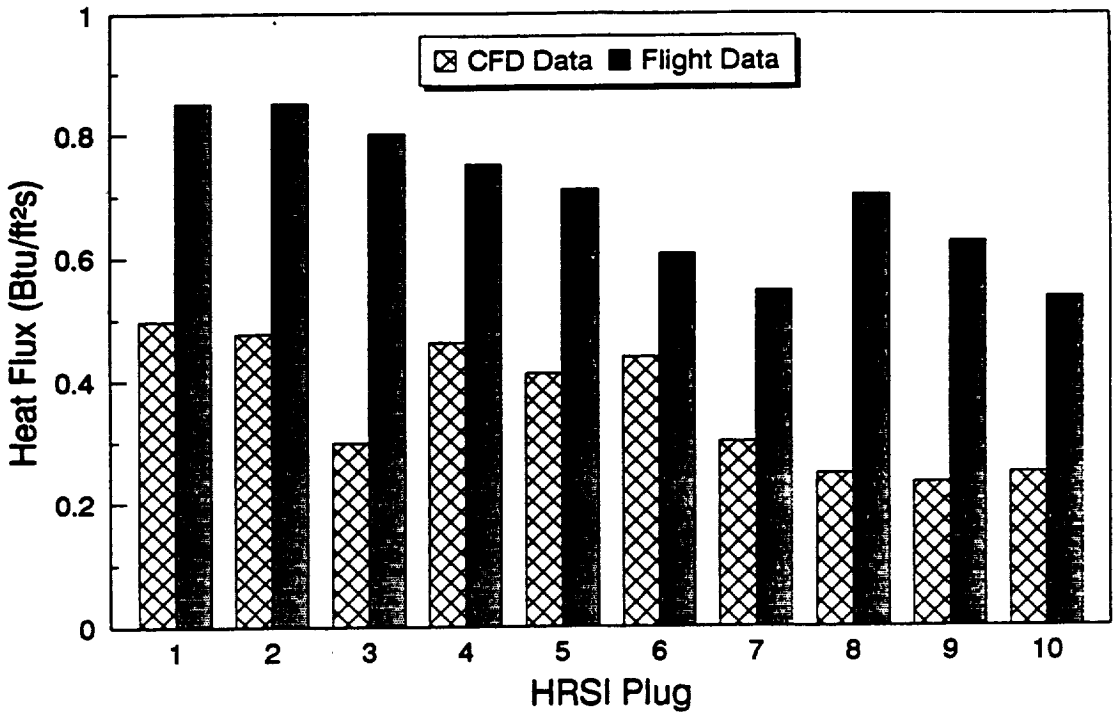

Figure 7. Heat flux at HRSI plugs, Mach 3.52, $\alpha = 7.35°$, flight 001.

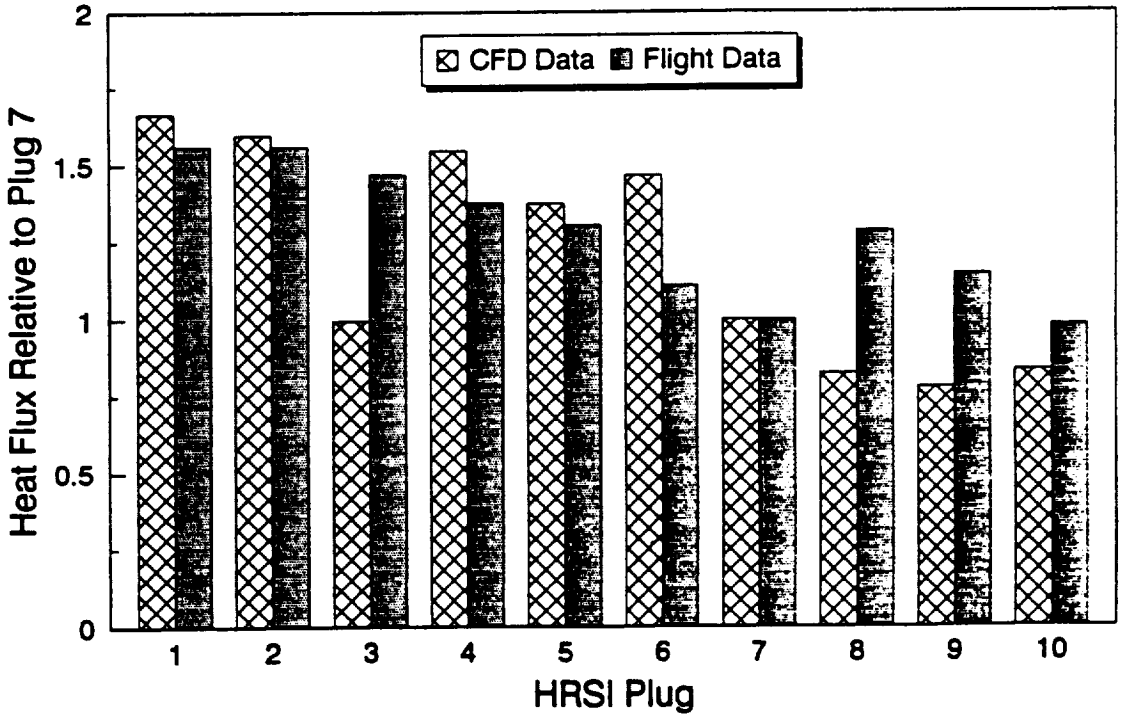

Figure 8. Relative heat flux at HRSI plugs, Mach 3.52, $\alpha = 7.35°$, flight 001.

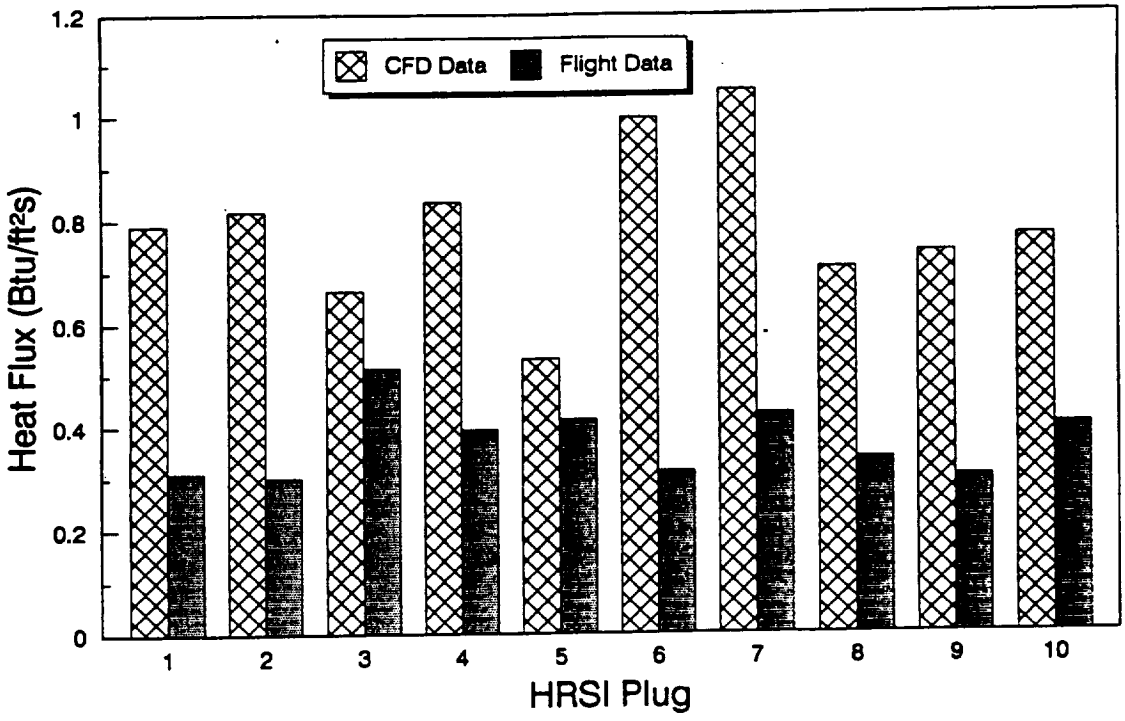

Figure 9. Heat flux at HRSI plugs, Mach 6.67, $\alpha = 0^{\circ}$, flight 001.

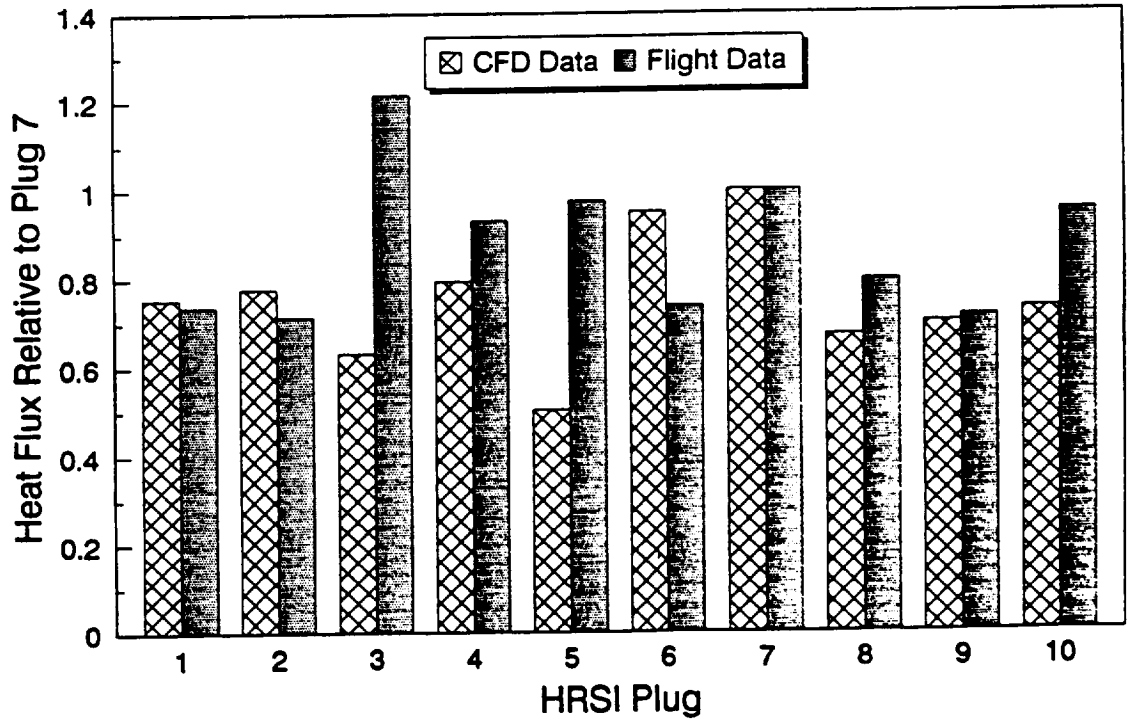

Figure 10. Relative heat flux at HRSI plugs, Mach 6.67, $\alpha = 0^{\circ}$, flight 001.

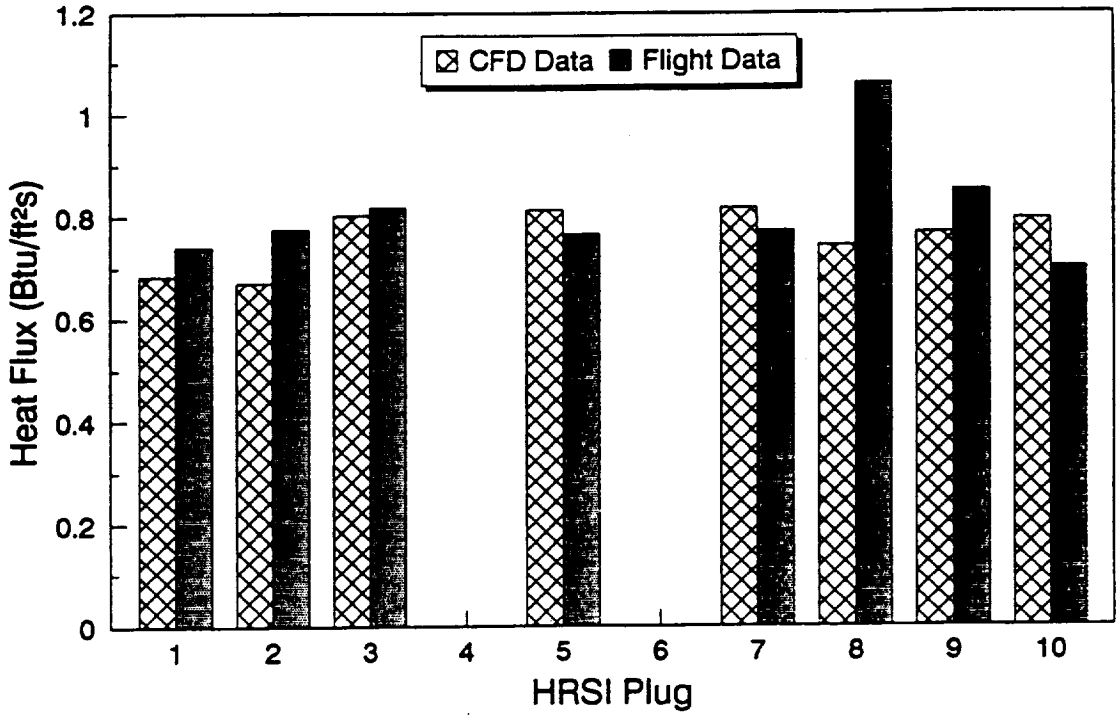

Figure 11. Heat flux at HRSI plugs, Mach 3.52, $\alpha = 2.65^{\circ}$, flight 002.

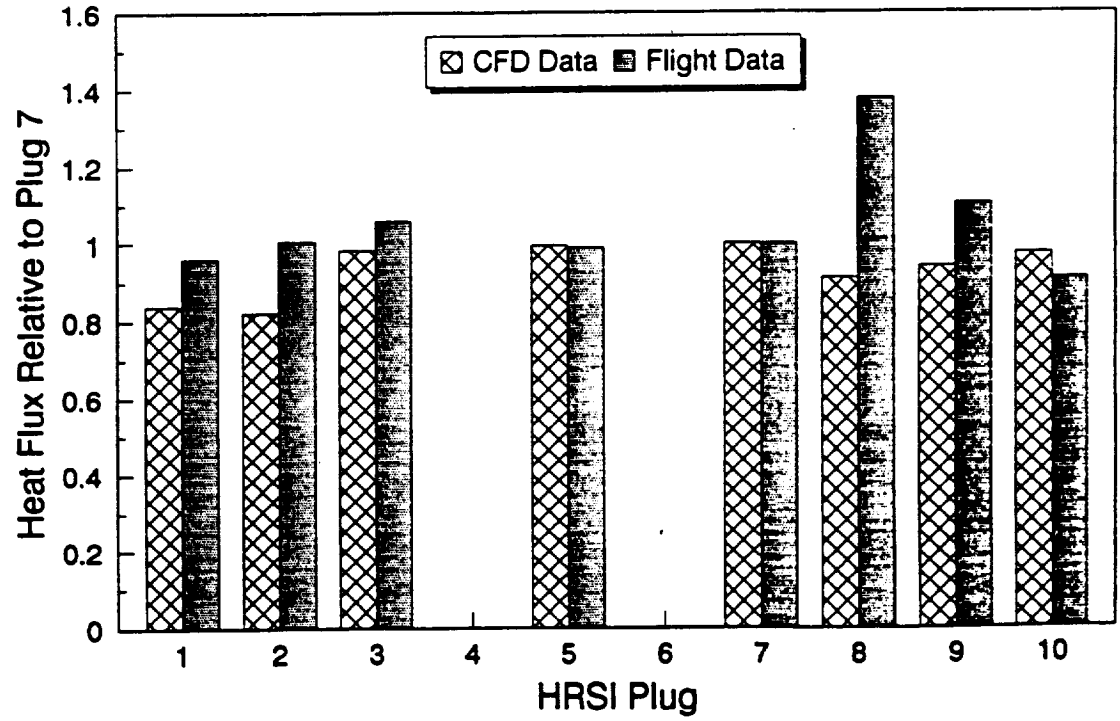

Figure 12. Relative heat flux at HRSI plugs, Mach 3.52, $\alpha = 2.65^{\circ}$, flight 002.

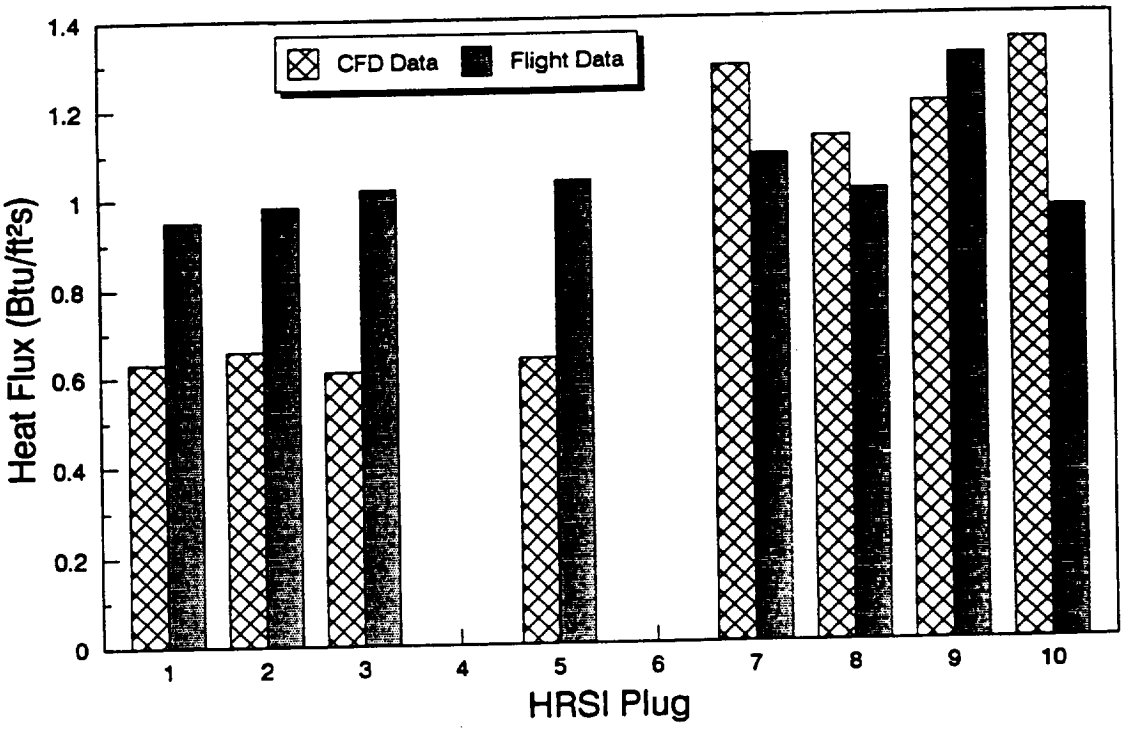

Figure 13. Heat flux at HRSI plugs, Mach 5.0, $\alpha = 0.5^{\circ}$, flight 002.

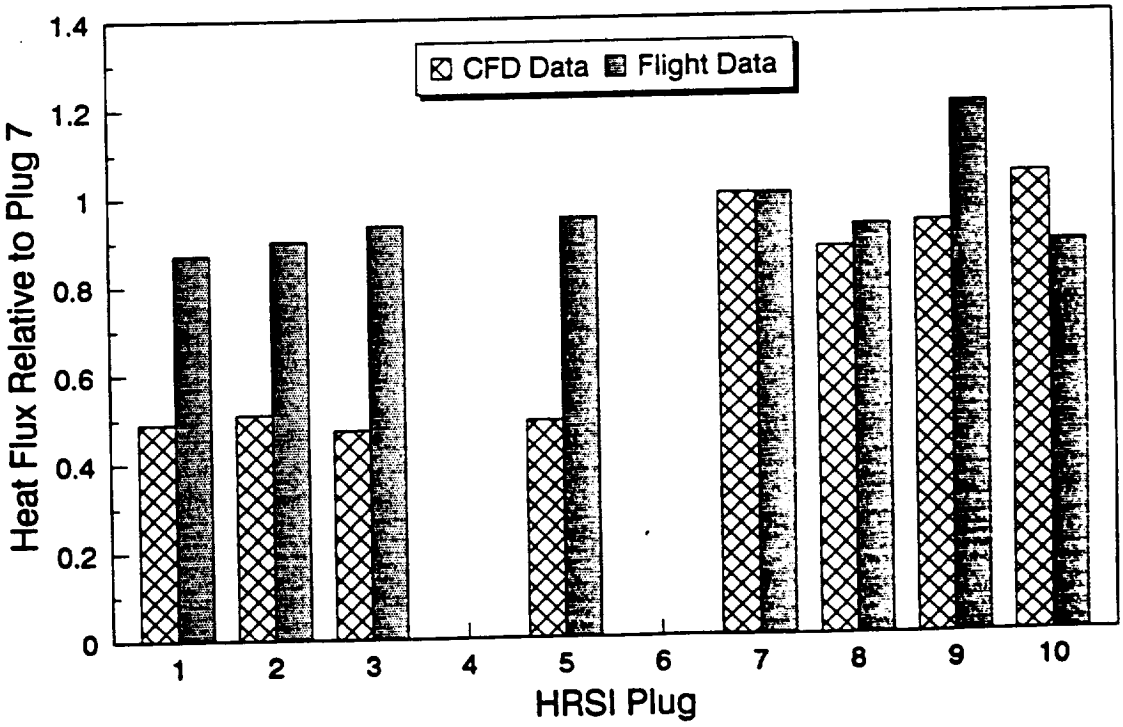

Figure 14. Relative heat flux at HRSI plugs, Mach 5.0, $\alpha = 0.5^{\circ}$, flight 002.

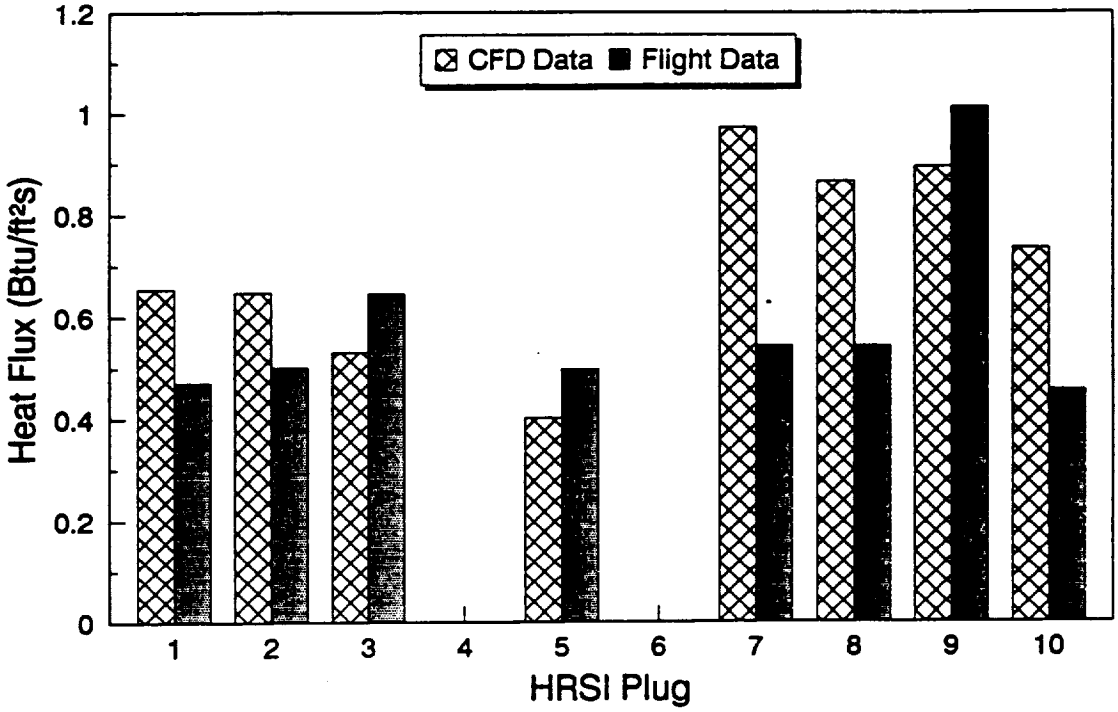

Figure 15. Heat flux at HRSI plugs, Mach 6.67, $\alpha = 0°$, flight 002.

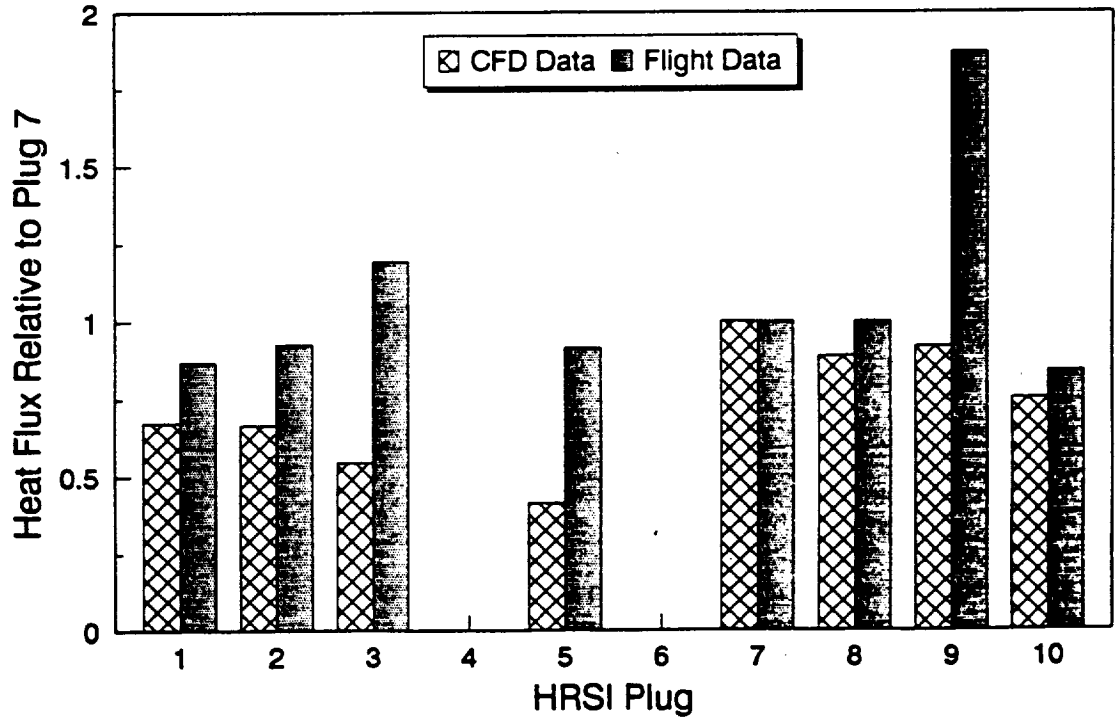

Figure 16. Relative heat flux at HRSI plugs, Mach 6.67, $\alpha = 0°$, flight 002.

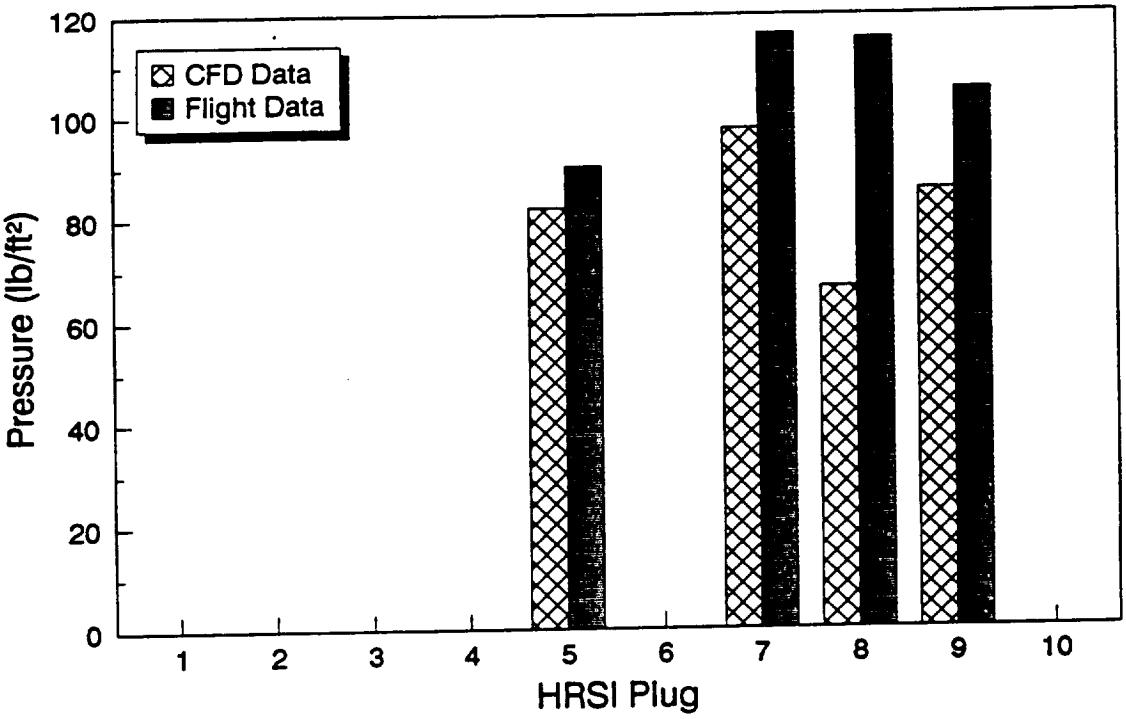

Figure 17. Pressure at HRSI plugs, Mach 3.52, $\alpha = 2.65°$, flight 002.

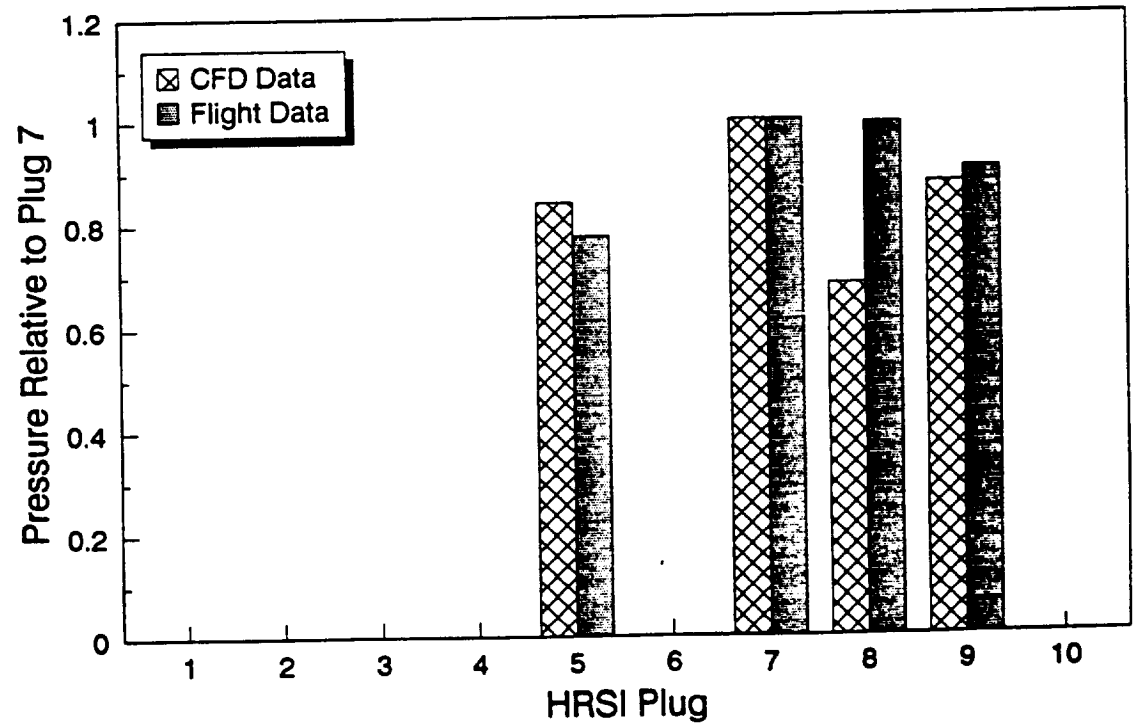

Figure 18. Relative pressure at HRSI plugs, Mach 3.52, $\alpha = 2.65°$, flight 002.

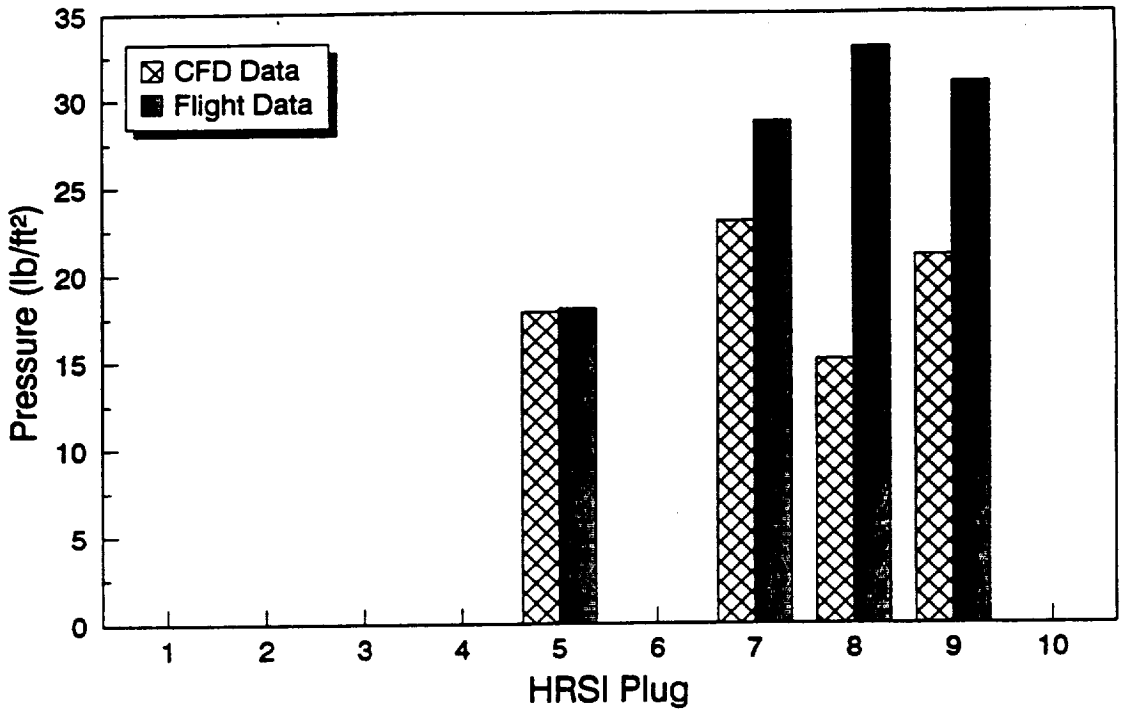

Figure 19. Pressure at HRSI plugs, Mach 5.0, $\alpha = 0.5^{\circ}$, flight 002.

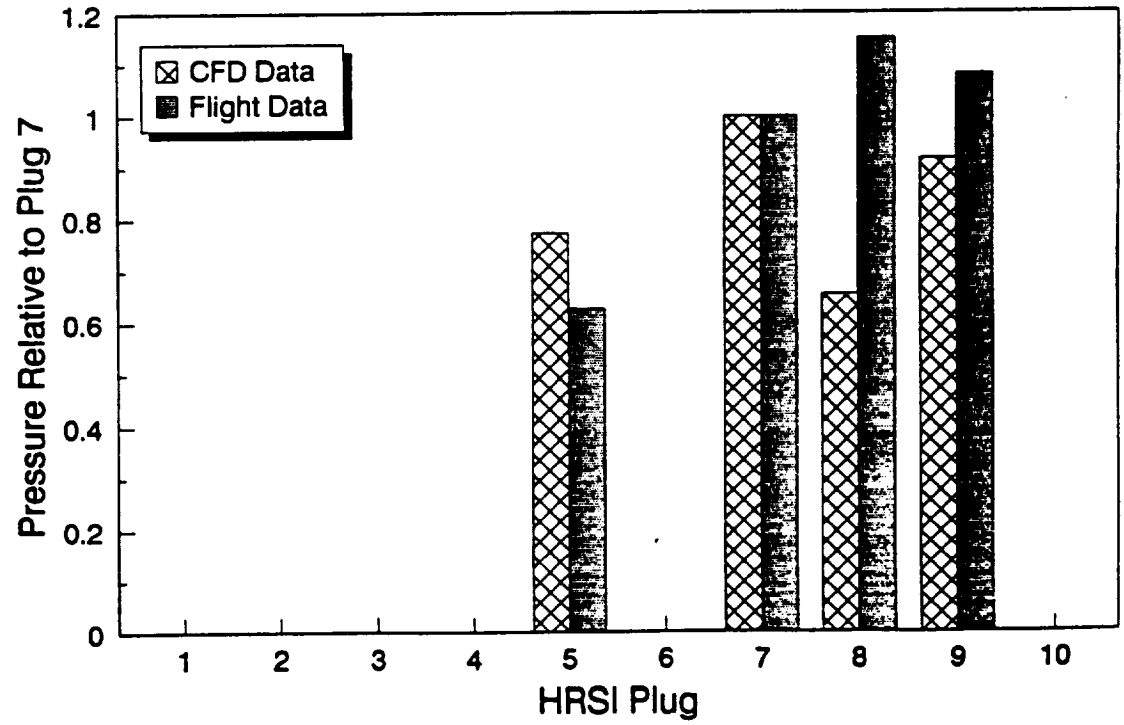

Figure 20. Relative pressure at HRSI plugs, Mach 5.0, $\alpha = 0.5^{\circ}$, flight 002.

REPORT DOCUMENTATION PAGE

Form Approved
OMB No. 0704-0188

1. AGENCY USE ONLY *(Leave blank)*	2. REPORT DATE	3. REPORT TYPE AND DATES COVERED
	August 1992	Contractor Report

4. TITLE AND SUBTITLE

A Computational Fluid Dynamics Analysis of the Hypersonic Flights of Pegasus®

5. FUNDING NUMBERS

WU-505-59-40
NCC 2-374

6. AUTHOR(S)

Darren Fricker, John Mendoza, and Ivan Catton

7. PERFORMING ORGANIZATION NAME(S) AND ADDRESS(ES)

University of California, Los Angeles
405 Hilgard Avenue
Los Angeles, CA 90024

8. PERFORMING ORGANIZATION REPORT NUMBER

H-1835

9. SPONSORING/MONITORING AGENCY NAME(S) AND ADDRESS(ES)

NASA Dryden Flight Research Facility
P.O. Box 273
Edwards, CA 93523-0273

10. SPONSORING/MONITORING AGENCY REPORT NUMBER

NASA CR-186023

11. SUPPLEMENTARY NOTES

NASA technical monitor was Robert Curry, NASA Dryden Flight Research Facility.

12a. DISTRIBUTION/AVAILABILITY STATEMENT

Unclassified — Unlimited
Subject Category 34

12b. DISTRIBUTION CODE

13. ABSTRACT ***(Maximum 200 words)***

The performance of a fully viscous, three-dimensional Navier-Stokes solver, PARC3D, was tested. The criteria for judging the performance of the CFD code were based on flight data from the first two flights of the Pegasus.® The flight data consisted of heat-transfer rates and sparse pressure coefficients primarily in the fillet region of the vehicle. The code performed remarkably well in all aspects of the tests. As expected, the best heat-transfer results were obtained for the low Mach number simulations. These results are attributed to lack of high ablation rates at the lower Mach numbers since the CFD simulations did not account for ablation at the vehicle surface. As the Mach number increased, the ablative effects became more apparent in the comparisons. This effect was evident at the highest Mach numbers, when PARC3D would consistently overpredict the aerothermal heat flux. To evaluate the code thoroughly, flight data would be required over the entire fillet region, rather than at a few discrete locations. In this manner, CFD heat-flux profiles could be accurately evaluated. Although the pressure data were sparse, the trends suggest that the code predicts surface pressures with reasonable accuracy. Three of the four locations yield pressures that are consistent, but the CFD results yield pressures below the flight data by a factor of 2 at the fourth location.

®Pegasus is a registered trademark of Orbital Sciences Corp., Fairfax, Virginia.

14. SUBJECT TERMS	15. NUMBER OF PAGES
Pegasus; computational fluid dynamics; hypersonic flight	31
	16. PRICE CODE: A03

17. SECURITY CLASSIFICATION OF REPORT	18. SECURITY CLASSIFICATION OF THIS PAGE	19. SECURITY CLASSIFICATION OF ABSTRACT	20. LIMITATION OF ABSTRACT
Unclassified	Unclassified	Unclassified	Unlimited